Effect of nanoparticle polydispersity on the self-assembly of polymer tethered nanospheres

Carolyn L. Phillips and Sharon C. Glotzer

Citation: J. Chem. Phys. **137**, 104901 (2012); doi: 10.1063/1.4748817
View online: http://dx.doi.org/10.1063/1.4748817
View Table of Contents: http://jcp.aip.org/resource/1/JCPSA6/v137/i10
Published by the American Institute of Physics.

Effect of nanoparticle polydispersity on the self-assembly of polymer tethered nanospheres

Carolyn L. Phillips[1,a)] and Sharon C. Glotzer[1,2,b)]
[1]*Applied Physics Program, University of Michigan, Ann Arbor, Michigan 48109, USA*
[2]*Department of Chemical Engineering and Department of Materials Science and Engineering, University of Michigan, Ann Arbor, Michigan 48109, USA*

(Received 23 December 2011; accepted 14 August 2012; published online 10 September 2012)

Recent simulations predict that aggregating nanospheres functionalized with polymer "tethers" can self-assemble to form a cylinder, perforated lamellae, lamellae, and even the double gyroid phase, which are phases also seen in block copolymer and surfactant systems. Nanoparticle size polydispersity is likely to be a characteristic of these systems. If too high, polydispersity may destabilize a phase. Using multiple thermodynamic paths to explore the phase diagram as a function of temperature and polydispersity, we explore the effect of nanosphere size polydispersity on the phase diagram. We show that in the portions of the phase diagram characterized by an icosahedral local nanoparticle packing motif, a low amount of polydispersity lowers the energy and a large amount of polydispersity raises the energy of the system by disrupting the icosahedral packing. In general, regions of the phase diagram characterized by liquid-like icosahedral packing have high terminal polydispersities from 15% to more than 30%. In the regions of the phase diagram characterized by crystalline local packing, polydispersity raises the energy of the system and induces a phase transition from crystalline to liquid-like ordering within the nanosphere rich regions of the microphase. We find the bilayer crystalline lamellae phase has a terminal polydispersity of 6%, but may still be partially crystalline up to 12%. © *2012 American Institute of Physics*. [http://dx.doi.org/10.1063/1.4748817]

I. INTRODUCTION

The ability of block copolymers to phase separate into periodic micro-domains makes them attractive building blocks for engineering self-assembled nanomaterials.[1–3] Possible applications of the periodic nanometer-sized domains include microelectronics[4] and high-density storage media,[5] photonic bandgap materials,[6,7] and drug delivery systems.[8,9] Recent attention has focused on the use of polymer-tethered nanoparticles as a means to create novel nanomaterials by exploiting the block copolymer-like immiscibility between nanoparticle and tether.[10–16] Several techniques exist to create composite polymer-nanoparticles. Westenhoff and Kotov, for example, used poly(ethyleneglycole) PEG polymer to tether a CdTe nanoparticle to a surface.[17] Several groups have created gold or SiO_2 nanoparticles functionalized with polymers or DNA linkers.[18–20] Even more advanced techniques are being proposed to create nanoparticles with multiple functionalizations with controlled placements for creating self-assembled structures.[21,22] Polymer tethered nanosphere amphiphiles[10] are thus currently realizable.

Iacovella and co-workers[23–25] predicted using computer simulations that polymer-tethered nanospheres (NS) (Fig. 1) form, under suitable conditions, phases similar to block copolymers.[26–28] The ordered phases found when the NS head group is in poor solvent are hexagonally packed cylinders (H), the double gyroid (DG), perforated lamellae (PLH), and lamellar bilayers (L), as shown in Figures 2–4. At temperatures outside the stability range of these phases the tethered nanoparticles still aggregate, but no ordered structure is found. This region is characterized by disordered wormy micelles (DWM).

The phase diagram predicted by Iacovella *et al.* was based on monodisperse tethered nanospheres (TNS) with uniform diameter NS. In all nanoparticle synthesis approaches, the polydispersity is non-zero, and in some cases can be appreciable. State-of-the-art techniques are able to achieve nanoparticles with polydispersity values as low as 6%.[29–31] For other self-assembling liquid crystal or hard sphere systems, it has been recognized that certain crystalline orderings can only tolerate a certain level of polydispersity and still be a stable phase; that is, they exhibit terminal polydispersity.[32] For example, Pusey[33] argued that crystallization of hard sphere colloids would have a terminal polydispersity between 6% and 11%, a range supported by subsequent experiments.[34] Terminal polydispersity for different systems has been studied experimentally,[35] analytically,[36] and computationally.[32,37]

In prior work,[38] we considered the impact of polydispersity on the DG phase of the TNS phase diagram. The DG (Fig. 3) is a triply periodic structure of space group Ia3d where space is divided into three regions: two interpenetrating but identical networks (here, the NS domain) and a matrix (polymer tether domain). For the monodispese TNS system considered, the phase is found in only a small region of the phase diagram. Phillips *et al.* found the DG phase may have no terminal polydispersity, but that the phase may be increasingly kinetically inhibited from forming for polydispersities higher than 10%. We now consider how

a)Present address: Computation Institute, Argonne National Laboratory, Lemont, Illinois 60439, USA.
b)sglotzer@umich.edu.

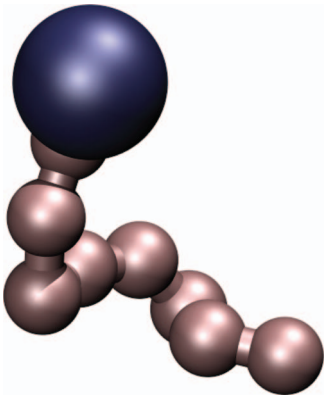

FIG. 1. A polymer functionalized nanosphere of diameter 2. The polymer is modeled as 8 soft sphere (WCA) beads connected by FENE springs.

polydispersity affects all the ordered phases of the phase diagram of the tethered nanosphere system. We consider, for example, how polydispersity influences the order-disorder temperature T^*_{ODT} between the DWM phase and ordered phases, and whether, beyond a "terminal polydispersity," a different phase may be stabilized. We are also interested in how increasing polydispersity affects internal properties of the phase, such as the local packing structure and packing fraction. Understanding the influence of polydispersity on these properties may explain why phases become stabilized or destabilized by increasing polydispersity, and provide insight into the internal structure of materials created from polydisperse TNS.

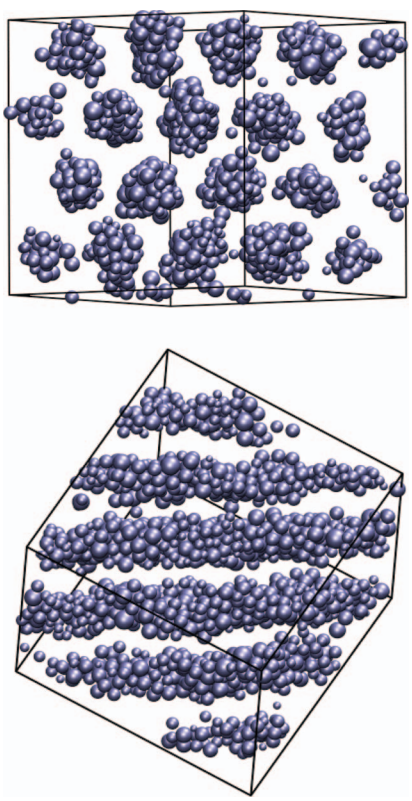

FIG. 2. Two views of a simulation cell containing 2000 TNS in the H phase. NS are blue; Tethers are not shown. The NS in this system have polydispersity $\Delta = 20\%$.

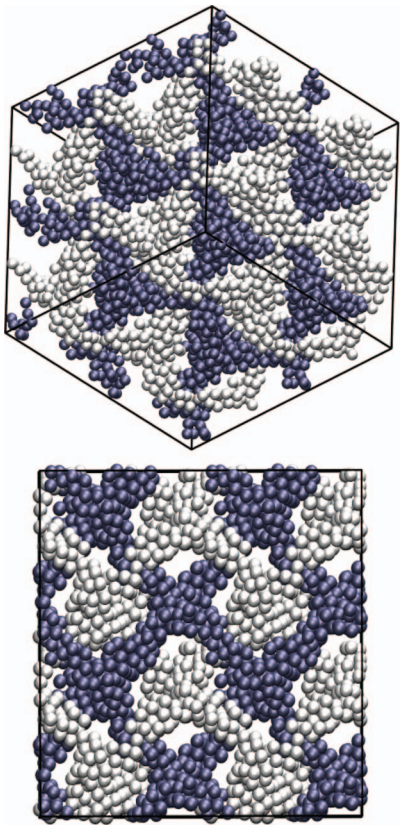

FIG. 3. The top panel shows 8 unit cells of a double gyroid (DG) phase. The NS are monodisperse and shown in blue and white. Tethers are not shown. The bottom panel shows the same 8 unit cells from a side perspective.

In Phillips *et al.*,[38] analysis of phase stability was based on using two separate "paths" through the phase diagram to identify the stable state. For one path, the system is initialized and equilibrated at a high temperature to a random disordered state. The simulation is then cooled and re-equilibrated at the new temperature. Ordered phases that form at a given temperature via different cooling schedules represent free energy minima. This "path" through the phase diagram resembles actual self-assembly of a physical system, albeit using a cooling schedule that is likely accelerated by several orders of magnitude relative to a physical system. This path shall be subsequently referred to as the conventional path (CP). The second path, introduced in Phillips *et al.*,[38] considers polydispersity as a perturbation to the monodisperse state. Polydispersity is introduced to a monodisperse ordered phase by "growing" the NS to a target diameter distribution, while at low temperature. The system is then heated and equilibrated to determine if the phase remains stable. This path shall be subsequently referred to as the alternate path (AP).

In the thermodynamic limit, these two "paths" through the phase diagram should produce identical free energy minima. In practice, however, at state points where both a disordered arrangement and an ordered arrangement may locally minimize the free energy, the CP is biased towards being kinetically trapped in the disordered phase and the AP is biased towards being kinetically trapped in the ordered phase. Further analytical tools would be required to determine which of the two phases minimizes the free energy globally, and which

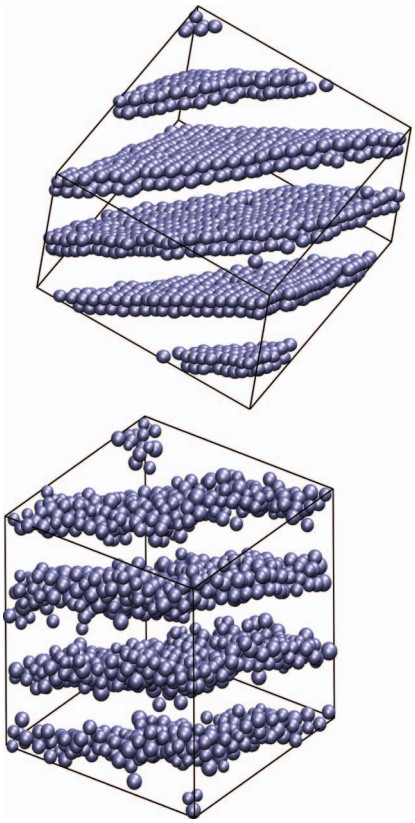

FIG. 4. The top panel shows 2000 TNS that have self-assembled to the L phase by a conventional path. The NS in this system have polydispersity $\Delta = 3\%$. The bottom panel shows 2000 TNS that have self-assembled to the PLH phase by an alternate path. The NS in this system have polydispersity $\Delta = 10\%$.

represents a metastable phase. Thus, we use these two paths in this paper to bound the possible phase diagrams of the TNS system subject to polydispersity.

Phillips *et al.*[38] also introduced using a quasi-equilibrated system to generate continuous functions characterizing the influence of polydispersity on properties of the system, such as potential energy, packing fraction, packing structure, and coordination, and applied this to the DG phase. In this paper, we apply this method to the entire phase diagram to evaluate how different regions of the phase diagram are affected by polydispersity.

In Sec. II of this paper, we describe the method we use to model polydisperse TNS and how the polydispersity of a system can be changed continuously in a molecular dynamics simulation. We describe the analytical techniques we use to study the packing properties of polydisperse nanospheres, namely (1) the R_{YLM} structure analysis used to identify the local ordering of particles within the phase, and (2) the radical tessellation used to identify how increasing the polydispersity affects the net packing of nanospheres. In Sec. III, we present the results of our simulations and analysis. In subsection III A, we compare the phase diagrams generated by CP and AP. In subsection III B, we consider how properties of the system, such as internal structure, packing fraction, potential energy, and coordination number, are affected by polydispersity. In Sec. IV, we discuss the differences between the CP and AP phase diagrams for a volume fraction of $\phi = 0.4$, where the L phase is found in the monodisperse system. In Sec. V, we provide concluding remarks.

II. METHOD

Here, we briefly describe the simulation method and analysis method used. More technical details can be found in Appendices A and B.

A. Simulation method

We utilize a minimal coarse-grained molecular model to study the phase behavior of tethered NS, the same model used previously in studies of TNS.[24,38] NS are modeled as beads with average diameter 2.0σ connected to tethers via a finitely extensible non-linear elastic (FENE) spring.[39] Tethers are modeled as bead-spring chains containing eight beads of diameter σ connected via FENE springs. An example TNS is shown in Figure 1. Interactions between beads and NS are modeled using empirical pair potentials. The attraction between two nanoparticles of diameters d_i and d_j is modeled using a radially shifted 12-6 Lennard-Jones potential (LJ). Tethers interact via a purely repulsive Weeks-Chandler-Andersen (WCA) soft-sphere potential.[40] NS-tether interactions are also treated with the purely repulsive WCA soft-sphere potential. The model captures the geometry of the nanoparticles, immiscibility between tether and nanoparticles, and flexibility of the polymer tether.

We use Brownian dynamics (BD) to simulate the assembly of the TNS. The use of this method is described in detail in Refs. 10, 23, and 25. In BD, each bead is subjected to conservative, random, and drag forces, and its motion is governed by the Langevin equation. Bulk system volume fraction, ϕ, is defined as the ratio of volume of the beads to the system volume.

A set of polydisperse NS is created by sampling from a Gaussian distribution of particle diameters d. The non-dimensionalized polydispersity, Δ, is defined as $100\delta/\bar{d}$, where δ is the standard deviation and $\bar{d}$ is the average diameter of the distribution. Since any simulation contains a finite set of NS drawn from this distribution, the nominal polydispersity of the distribution, i.e., the polydispersity of the distribution being sampled, and the actual polydispersity of the set generated differ slightly. In this paper, the nominal polydispersity of the distribution is presented as an integer value. When the polydispersity has a decimal component, this represents the actual polydispersity of the distribution. Polydispersity values reported on plots are actual Δ values.

At a given volume fraction, ϕ, we explore the $T^* - \Delta$ phase diagram by changing the variables of temperature T^* and polydispersity Δ. All simulations are initiated at a high temperature disordered monodisperse NS state. Temperature is changed by resetting the BD thermostat or (equivalently) by resetting the ϵ pair interaction parameter to change T^* a small amount and then permitting the system to relax to its local equilibrium. To change the polydispersity, the diameters of every particle in the system is adjusted only a small amount per time step to prevent high energy particle overlaps from occurring. Also, at each time step, the net volume of all the particles is kept fixed so ϕ remains constant as Δ is changed.

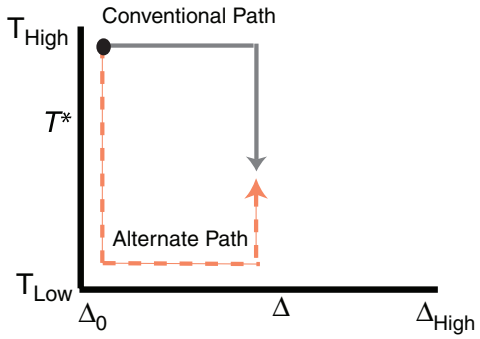

FIG. 5. Schematic showing the two paths, the conventional path (CP) and the alternate path (AP), used in the present study.

Upper and lower bounds are established for the order-disorder temperature, T^*_{ODT}, and the terminal value of Δ for ordered phases on a polydispersity vs. temperature phase diagram by using different thermodynamic paths, (CP and AP). A diagram of an example of a CP and AP is shown in Figure 5.

In some simulations, we study Δ as a continuous variable, for a fixed ϕ and T^*, by continuously adding or removing polydispersity to the NS extremely slowly, or quasistatically, while measuring properties of the system. The polydispersity is changed slowly enough that the system is able to relax in response to the change and the properties of the system (barring kinetically trapped phase transition regions), calculated as a function of time, closely approximate those of the equilibrated system. A diagram of an example path of this type is shown in Figure 6. The properties calculated when the polydispersity is increasing are labeled QE$\Delta\uparrow$ and the properties calculated as polydispersity is decreasing are labeled QE$\Delta\downarrow$.

In the thermodynamic limit, all the "paths" through the phase diagram should produce identical free energy minima. In practice, however, at state points where both a disordered arrangement and an ordered arrangement may locally minimize the free energy, the CP is biased towards being kinetically trapped in the disordered phase and the AP is biased towards being kinetically trapped in the ordered phase. Similar hysteresis is found between QE$\Delta\uparrow$ and QE$\Delta\downarrow$.

We introduce these different paths to try to circumvent the ergodicity issues of a finite simulation time. The AP, although non-physical, is akin to methods used in semigrand ensemble Monte Carlo simulations where the identity

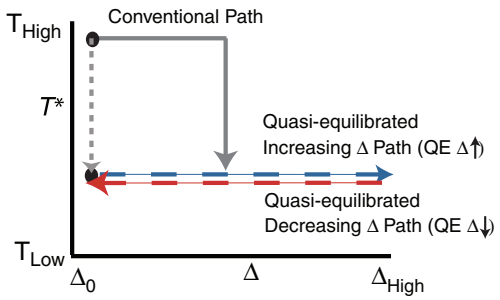

FIG. 6. Schematic of paths used in determining the quasiequilibration properties of polydispersity.

of each particle is allowed to change via a "ghost-growing procedure,[32,41] or even the use of a pivot cluster algorithm for non-local moves.[42]

B. R_{YLM} local structure analysis

To analyze the local ordering configurations of the nanospheres, we performed the R_{YLM} local structure analysis first introduced in Iacovella *et al.*[24] and further discussed in Refs. 25 and 38. The R_{YLM} method relies on creating a rotationally invariant spherical harmonic fingerprint of the central particle of a cluster of particles (for harmonics $l = 4$, 6, 12) and then matching this fingerprint to a library of known structures. For our system, the local packing of nanospheres is divided into clusters by grouping each NS and its nearest-neighbor nanospheres. The structure of each cluster is characterized by the family, namely, icosahedral, crystalline, or disordered, to which it matches best. This is used to analyze the local structure of a phase.

C. Packing density and coordination

We use the radical tessellation to examine packing density (compactness) and nearest neighbor trends in the micro-segregated head group NS domain, as opposed to the tether domain, as a function of polydispersity of the NS. For a given snapshot of the simulation, the radical tessellation divides the space into a polyhedral mesh whereby each bead in the simulation has an associated polyhedral radical cell. The packing fraction of the NS is measured by dividing the volume of all the NS by the volume of all the radical cells containing NS. We also use the radical tessellation to measure the local coordination or neighbor shell of each NS. We are interested only in the NS neighbors of a NS, and not the tether component, since the NS-NS interaction represents the important energetic interaction in the cooled system.[38] Two NS are considered to be neighbors if the radical cells of the two nanospheres share a facet. We use this definition to calculate how the system average NS coordination number is affected by polydispersity.

D. Computer resources

Simulations used locally authored code and the GPU-based HOOMD-blue code package under development in our group, which permitted rapid exploration of the phase diagram. The HOOMD simulations were run using our GPU cluster at the University of Michigan and the 32-node GPU cluster, AC, at the National Center for Supercomputing Applications on NVIDIA Tesla S1070s. Simulations using our CPU-based code were run on 2.0 GHz G5 nodes at the University of Michigan and 2.2 GHz Opteron Nodes (Jacquard Cluster at National Energy Research Scientific Computing Center).

III. RESULTS

A. CP and AP phase diagrams

To determine the impact of Δ on the TNS phase diagram, the system was studied at volume fractions that represent each

of the self-assembled phases of the monodisperse TNS system studied in Iacovella *et al.*,[24] or the H, DG, PLH, and L phases. A volume fraction of $\phi = 0.25$ was chosen to study the H phase. The PLH and L phases, for the monodisperse system, are found at the same volume fraction, but at different temperatures, so the volume fraction $\phi = 0.4$ was chosen to study both of these phases. Small investigations at nearby ϕ confirmed that the behavior of the phase at a single ϕ snapshot is generalizable to other volume fractions where the phase is present. In Phillips,[38] the DG phase was studied at $\phi = 0.3 \pm 0.015$. These results are provided for comparison. To generate the phase diagram, simulations of 505 and 2000 TNS (4545 and 18 000 particle simulations, respectively) were simulated for $\phi = 0.25$ and 0.4. For the H phase, nominal polydispersities of $\Delta = 0\%$, 10%, 20%, and 30% were considered. For the L and PLH phases, nominal polydispersities of $\Delta = 0\%$, 3%, 4%, 5%, 6%, 7%, 8%, 9%, 10%, 11%, 12%, 20%, and 30% were considered. For each nominal polydispersity, a minimum of 5 different random NS diameter distributions were considered. In Phillips *et al.*,[38] the DG phase was considered at nominal polydisperties of $\Delta = 0\%$, 2%, 4%, 5%, 6%, 8%, 10%, 12%, 14%, 15%, 16%, 18%, 20%, 24%, 25%, and 30 % and for $0.285 \leq \phi \leq 0.315$, or 5% above and below where the DG phase was found for the monodisperse case in Iacovella *et al.*[24] These results are provided for comparison to the rest of the phase diagram.

For the CP and AP phase diagrams, a "phase" was considered stable if the phase persisted for a minimum of 10×10^6 time steps. For parts of the phase diagram where the AP and CP phase diagrams differed, this criteria was extended to 100×10^6 time steps.

Using the CP method to generate a phase diagram, a single phase is almost never exclusively found at a state point due to kinetics and metastability. At each volume fraction where an ordered phase is found, some fraction of the simulations become kinetically trapped in disordered states or ordered phases with defects (e.g., screw dislocations, non-ordered connections between the cylinders or layers). For the DG phase, which exists in a small region of the phase diagram, close to both the H, PLH, and L phases, some fraction of the simulations produce the neighboring phases, or even an intermediate phase with planar connections between the hexagonally packed cylinders. In the thermodynamic limit, we would expect only a single phase to be present. In Figures 7 and 8, the CP phase diagrams show the most ordered phase found at each state point, where the H and PLH phases are considered more ordered than DWM, L is considered more ordered than PLH, and DG is considered more ordered than H, L, or PLH. The likelihood of forming the DG phase using a CP was found to be a strong function of polydispersity. Therefore, extra consideration is given to the frequency of finding the DG phase relative to polydispersity in determining an "effective" terminal polydispersity.

Using the AP method, a single phase is almost always found at a given state point. The only exception is close to the order-disorder temperature T^*_{ODT} where a small amount of deviation in T^*_{ODT} of individual simulations may occur. This uniformity is a natural consequence of initializing the simulation in the assumed ordered state for a given T^*, ϕ, and Δ. In Figures 7 and 8, the AP phase diagram shows the least ordered state found at each state point.

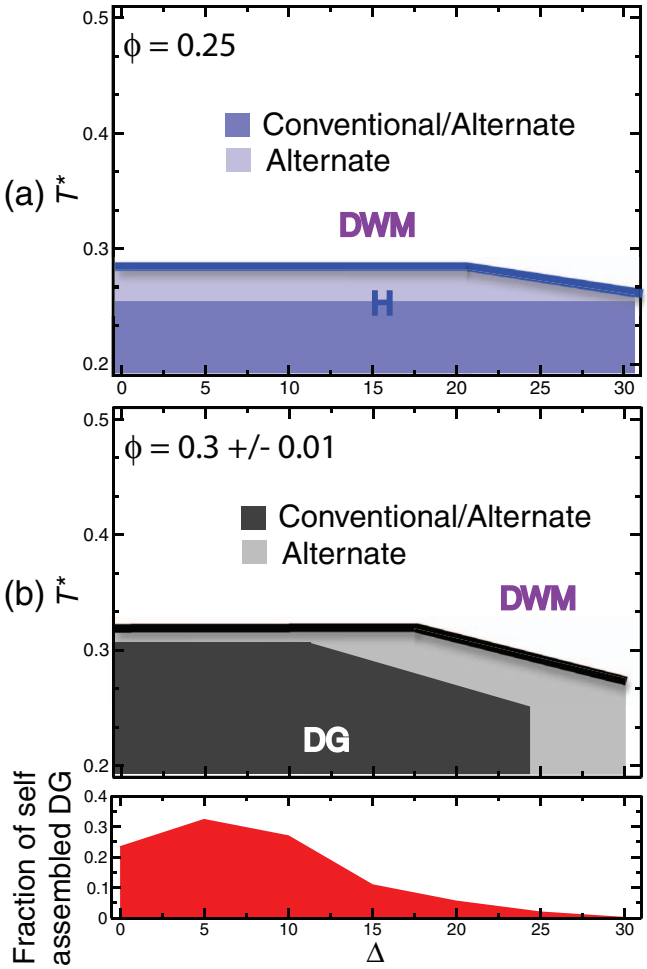

FIG. 7. The CP and AP phase diagrams (T^* versus Δ) are shown in overlay for the volume fraction $\phi = 0.25$ and $\phi = 0.3 \pm 0.01$. The region where the CP indicates the phases to be stable is contained within the region where the AP indicates the phase to be stable. Thus the darker shaded region is labeled both conventional and alternate. The bottom graph shows for DG the relative likelihood of the DG phase self-assembling via the CP as a function of polydispersity.

In Figure 7, the CP and AP phase diagrams (T^* versus Δ) are shown in overlay for the volume fraction $\phi = 0.25$ and $\phi = 0.3 \pm 0.01$. For both the H and DG phases, the region where the CP indicates the phases to be stable is contained within the region where the AP indicates the phase to be stable. Thus the darker shaded region is labeled both conventional and alternate.

Considering up to $\Delta = 30\%$, the H phase has no terminal polydispersity. However, the AP phase diagram indicates that for $\Delta \geq 20\%$, increasing Δ lowers T^*_{ODT}. From $\Delta = 20\%$–30%, T^*_{ODT} decreases from 0.28 to 0.25.

For the DG phase, the CP and AP phase diagrams indicate that increasing Δ lowers T^*_{ODT} for $\Delta > 10$ and $\Delta > 20\%$, respectively. The CP and AP phase diagrams show the DG phase to be stable up to $\Delta = 25\%$ and 30%, respectively. However, a study of DG formed by CP indicates that polydispersity can have significant impact on the likelihood of the DG phase forming.

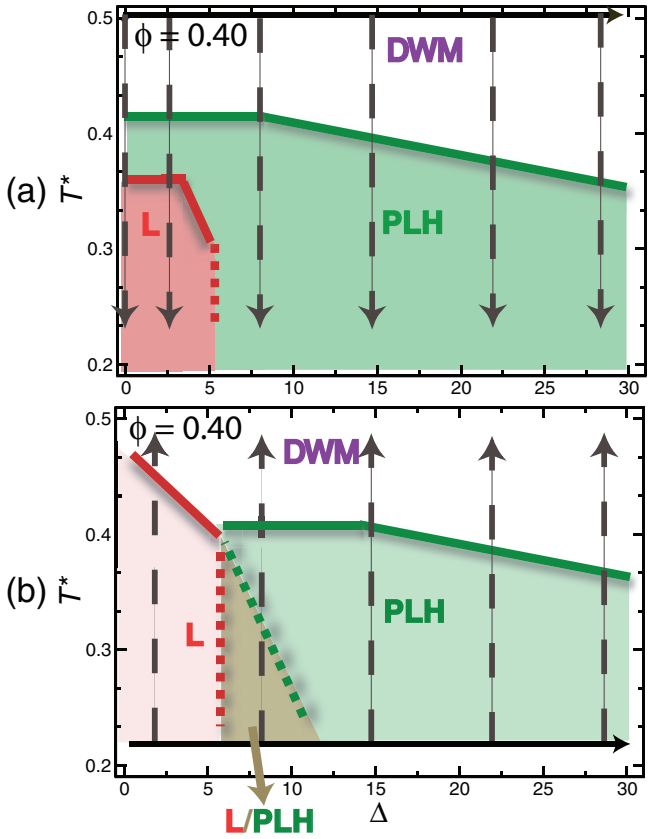

FIG. 8. The (a) CP and (b) AP phase diagrams (T^* versus Δ) are shown for the volume fraction $\phi = 0.4$. The arrows illustrate the path used to explore the phase diagram.

At the bottom of Figure 7(b), the relative likelihood of finding the DG phase at a given polydispersity is shown. This assessment is based on the survey of the likelihood of finding the DG phase for $\Delta = 0\%$–30% and $0.29 \leq \phi \leq 0.31$ in Ref. 38, Fig. 3. At each Δ and ϕ, 10 simulations were performed with a cooling schedule terminating at $T^* = 0.2$. Of the 350 total simulations, 56 formed the DG phase. The relative likelihood of finding the DG phase is determined by dividing the number of DG phases found in simulation at a given polydispersity by the total number of DG phases found in all simulations of Ref. 38 (see Fig. 3). The data are presented this way to separate the influence of polydispersity on formation of the DG phase from the general kinetic difficulty of forming the DG phase. As discussed in Ref. 38, a small amount of polydispersity ($\approx$5%) helps the DG to form, while for $\Delta > 10\%$, increasing Δ decreases the likelihood of the DG phase forming. For comparison, while fewer total independent simulations were considered for the CP-generated H and lamellar phases, the simulations consistently showed the likelihood of finding the two phases from 0% to 15% was the same as from 15% to 30%.

In Figure 8, the CP and AP phase diagrams for a TNS system of $\phi = 0.4$ are shown. Arrows indicating the path through the CP and AP phase diagrams are provided for illustration.

The CP phase diagram indicates that both the PLH and L phases are present at low Δ, at high and low temperatures, respectively, but that increasing Δ lowers T^*_{ODT} and that only PLH is found for $\Delta > 5\%$. Specifically, as found in Ref. 23 for the monodisperse system, the CP phase diagram indicates that for $0.375 \leq T^* \leq 0.4$, the PLH phase is present. For $T^* \leq 0.35$, the L phase is present. Over the range $3\% \leq \Delta \leq 5\%$, the T^*_{ODT} for the L phase decreases from 0.35 to 0.3. For $\Delta > 5\%$, the L phase is no longer present, and only the PLH phase is found. For $\Delta > 7\%$, the T^*_{ODT} for the PLH phase also decreases with increasing Δ.

In contrast, for the AP phase diagram, only the L phase is present for low Δ, while for intermediate levels of Δ, a coexistence phase is found at low temperatures and a PLH phase is found at higher temperatures. At high levels of Δ, only a PLH phase is present. Specifically, the AP phase diagram shows the L phase to be present for $T^* < 0.475$ at $\Delta = 0$. For increasing Δ, the T^*_{ODT} for the L phase decreases to 0.4. Between $\Delta = 6\%$ and 12%, at $T^* = 0.25$, the TNS system and the L and PLH phases are in coexistence (subsequently referred to as L/PLH), with an increasing fraction of the system in the PLH phase with increasing Δ. For $\Delta \geq 12\%$, only the PLH phase is present. For Δ increasing from 6% to 12%, the T^*_{ODT} of the coexistence region decreases from 0.4 to 0.25. For $\Delta > 15\%$, increasing Δ decreases the T^*_{ODT} of the PLH phase. The cause of the substantial difference between the CP and AP phase diagrams at $\phi = 0.4$ is discussed in Sec. IV.

A special concern for the AP phase diagram at $\phi = 0.4$ is that the starting point state for increasing the polydispersity of the NS is a crystal phase. For the H, DG, and PLH phase, the NS are diffusive. For the L phase, where the NS form a bilayer crystal, the NS usually stay fixed in a lattice position over the simulation and the individual system cannot explore different arrangements of NS. However, we find that by randomly distributing the growth schedules over the NS, the properties of one sampling is not measurably different from another. For example, there is no significant impact on phase boundaries found.

B. Polydispersity perturbation functions

As discussed in Ref. 38, the stability of a phase is affected by the potential energy of the NS packing, which is, in turn, affected by the average number of NS neighbors, or coordination number, and packing fraction of the phase. Therefore, we are interested in understanding how polydispersity influences these properties. We are also interested in characterizing the composition of local NS ordering (e.g., crystalline vs icosahedral) as a function of Δ. For example, in Ref. 38, we concluded that the increase in local icosahedral ordering at $\Delta = 6\%$–8% helped facilitate the formation of the DG phase. Also we are interested in characterizing the coexistence region in the AP phase diagram as a function of increasing Δ. To determine how polydispersity perturbs the properties of the monodisperse TNS system, we calculate the properties of a quasi-static system where polydispersity is first slowly increased (QE$\Delta\uparrow$) and then decreased (QE$\Delta\downarrow$).

Figure 9 shows how polydispersity perturbs the crystalline ordering (Fig. 9(a)), icosahedral ordering (Fig. 9(b)), potential energy (Fig. 9(c)) average coordination number (Fig. 9(d)), and packing fraction (Fig. 9(e)) of the TNS at

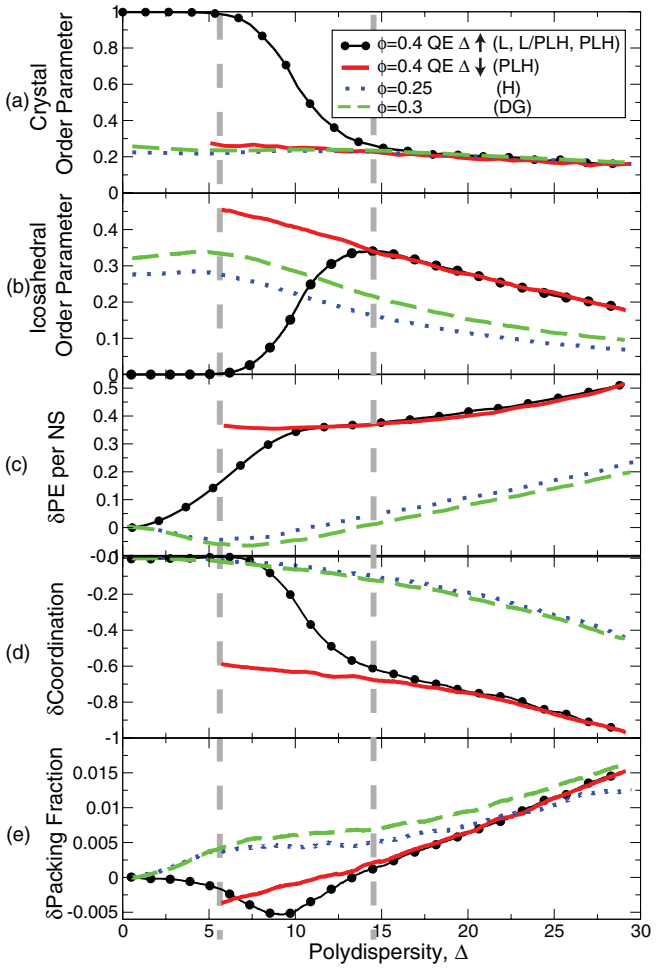

FIG. 9. The effect of polydispersity on (a) the crystalline vs (b) icosahedral local packing, (c) the potential energy of the NS-NS interaction, (d) the coordination, and (e) packing fraction of the particles, as determined by a radical tessellation, is compared at $\phi = 0.25$, 0.3, and 0.4. The phases found along each curve are indicated in parentheses in the legend. The dashed arrows indicate the collapse of QE$\Delta\downarrow$ data onto QE$\Delta\uparrow$ data at $\phi = 0.4$.

$\phi = 0.25$, 0.3, and 0.4, respectively. For potential energy, packing fraction, and coordination number, these properties are shown as the deviation or offset from the monodisperse system value. The potential energy is made an intensive property by scaling by the number of NS in the system.

We observed that for $\phi = 0.25$ and $\phi = 0.3$, the quasi-static paths, QE$\Delta\uparrow$ and QE$\Delta\downarrow$, have a minimal amount of hysteresis relative to each other. Also the systems remain in the H and DG phases, respectively, over the entire polydispersity range. Therefore, two paths have been combined for each property for $\phi = 0.25$ and 0.3 in Figure 9 and are represented as a blue dotted line and a green dashed line, respectively.

In contrast, a significant amount of hysteresis is present for $\phi = 0.4$ between the two quasi-static paths, QE$\Delta\uparrow$ and QE$\Delta\downarrow$ in the range between $6\% < \Delta < 14\%$. This region is indicated by the Δ range between the dashed lines in Figure 9. For $\phi = 0.4$, $\Delta < 6\%$ corresponds to the L phase, $\Delta > 14\%$ corresponds to the PLH phase, and in the range between $6\% < \Delta < 14\%$, QE$\Delta\uparrow$ corresponds to coexistence of L and PLH, while the QE$\Delta\downarrow$ corresponds to only PLH. For the QE$\Delta\downarrow$ path, for $\Delta < 5\%$, crystallization to the L phase occurs so slowly relative to the rate of decreasing the polydispersity, that the quasi-static method proves poor for generating statistics. Therefore, for QE$\Delta\downarrow$ $\Delta < 5\%$, data are not shown and, consequently, all QE$\Delta\downarrow$ data shown in Fig. 9 correspond to the PLH phase. The QE$\Delta\uparrow$ and QE$\Delta\downarrow$ paths are shown as a black line with circles and a solid red line, respectively.

From Figs. 9(a) and 9(b), we observe the local ordering of NS in the H, DG, and PLH phases is icosahedral. The degree of local icosahedral ordering is increased with increasing volume fraction, ϕ. For a fixed ϕ, the icosahedral ordering peaks at $\Delta = 6\%$ and then decreases with increasing polydispersity. The NS of the L phase ($\Delta < 6\%$) have a crystalline local ordering. These observations are consistent with Ref. 24, where Iacovella *et al.* divide the TNS phase diagram into two general regions, one characterized by liquid-like icosahedral NS packing, (i.e., DWM, H, DG, and PLH phases), with the fraction of icosahedral local ordering increasing with increasing ϕ, and a second characterized by crystalline NS packing region (L phase). These observations are also consistent with observation of Ref. 38 that a small amount of polydispersity promotes icosahedral ordering.

Between the grey dashed lines in Figs. 9(a) and 9(b) the continuous transition from primarily crystalline ordering to icosahedral ordering can be observed in QE$\Delta\uparrow$. The crystalline ordering decreases and the icosahedral ordering increases, indicating a Δ range of L and PLH coexistence. In Figure 10, snapshots of the system at $\phi = 0.4$ are shown in the coexistence region. NS that are identified as having a crystalline, icosahedral, and unidentified bond ordering by the R_{YLM} measure are colored red, dark blue, and light blue, respectively. As Δ increases from 0% to 12%, we observe the icosahedral/liquid regions emerging initially along grain boundaries and defects. At $\Delta = 10\%$, the crystal region has become an "island" in disordered PLH regions.

In Figures 9(c)–9(e), we see that the impact of Δ on system properties is primarily determined by the composition of the local packing structure, icosahedral or crystalline, as measured by Figures 9(a) and 9(b). The properties of phases with a liquid-like, icosahedral local ordering behave similarly upon an increase in Δ. Specifically, over any part of the range that any two curves share a local icosahedral ordering (e.g., all four curves for $\Delta > 14\%$) the offset potential energy, coordination, and packing fraction have nearly identical trends.

The potential energy and packing fraction of the crystalline L phase, when it is present, respond significantly different from the phases with icosahedral ordering. In Figure 9(c), the potential energy of the L phase rises with increasing Δ, $\Delta < 6\%$, even though the coordination of the TNS, per Fig. 9(d), is relatively invariant and even trending similar to the phases with icosahedral ordering. In Figure 9(e), increasing Δ causes the NS domain in the L phase to become less dense, or swell, thus causing the increase in the potential energy of the phase.

Properties of the coexistence phase behave as an average of the properties of icosahedral and crystalline phases, weighted by their proportional presence, with increasing Δ. In Fig. 9(d), the number of NS neighbors per NS decreases by 0.6 over the transition from crystalline to icosahedral

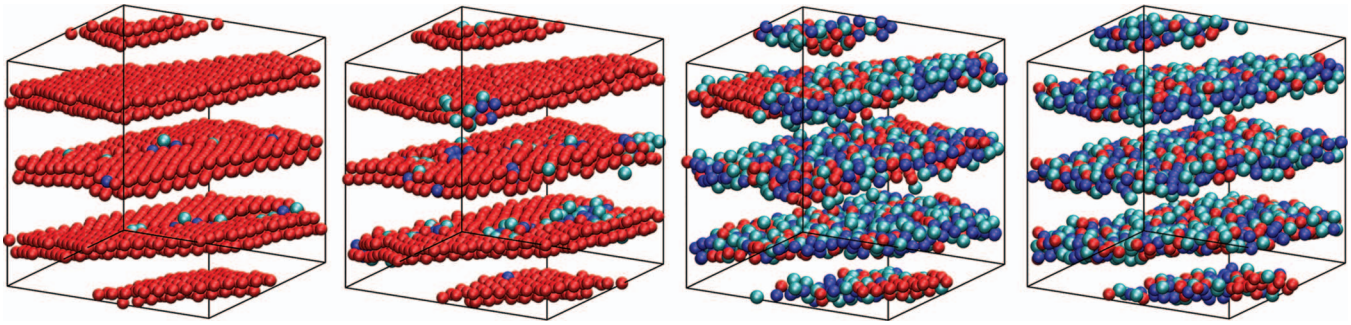

FIG. 10. A series of snapshots of the L phase is shown at polydispersity 0%, 6%, 10%, and 12% as polydispersity is grown into a monodisperse cooled system. At each polydispersity, the system was allowed to relax for 10×10^6 time steps. Nanospheres are colored red if locally crystalline, light blue if unidentifiable, and dark blue if icosahedral. Tethers are not shown. Initially, the system is in a totally crystalline state, with a few non-crystal NS found at grain boundaries and defects in the lamellae. At 6%, the system is still crystal, although the number non-crystal NS at grain boundaries and lamellae defects has increased. At 10%, the lamellae is mostly liquid and disordered, with a few small islands of crystal bilayer remaining. At 12%, the system is fully in the PLH phase. Note that although "red" particles are still present, they are not spatially correlated and represents the limitations of the identification algorithm.

local structure, while per Fig. 9(e), the phase is more densely packed at the end of the transition. Comparing the packing fraction of QE$\Delta\uparrow$ (L/PLH) to QE$\Delta\downarrow$ (PLH) between the grey dashed lines, it is apparent, first, that the PLH phase is denser than the L/PLH phase over this range, and second, that the onset of crystallization for the PLH phase is coincident with the two phases (L and PLH) approaching the same density.

IV. DISCUSSION

The impact of polydispersity on the bulk phase equilibria of hard discs,[42–44] soft discs,[45] hard spheres,[32,36,41,46–49] and soft spheres,[41,47,50] is an actively researched area in the study of colloids with many open contentious questions. Analysis of the phase diagram is complicated by features such as the coexistence of crystalline and amorphous phases, fractionation, where by different phases have different size dispersion or mean size, and the onset of glassy dynamics, that may explain the discrepancy between theory and experiment.

It is not immediately clear which system studied in bulk is most relevant to the TNS system. While the NS-NS interaction has a "soft repulsive term," the radial shifting of the potential creates a harder effective interaction, relative to particle diameter. The bilayer crystalline lamellar system has a combination of the characteristics of a two-dimensional and a three-dimensional system of spheres. It is strongly constrained in two directions parallel to the lamellar plane and softly constrained in the direction perpendicular to the lamellar plane. However, the bilayer lamella is also capable of reorienting inside the simulation cell (within limits) to relieve stress in the planar directions. Despite lacking a clear counterpart in bulk phase equilibria studies and despite that the methodology we used for studying TNS is not rigorous enough to directly contribute to the debate on the bulk phase equilibria, we remark that the results of this study are consistent with the more statistically rigorous studies of polydisperse hard spheres.

To summarize the results of several studies, the terminal polydispersity of a hard sphere crystalline phase has been shown to be 6%.[32,41,46,47] Above this polydispersity, a fluid may have two coexisting phases, a crystalline phase of low polydispersity and an amorphous phase of high polydispersity, if the kinetics of the system allow for fractionation to occur.[32,41,46,47,51] Above a polydispersity of 12% it has been proposed that the kinetics are highly suppressed,[48] explaining the lack of crystallites found in polydisperse fluids in experiment[34]

Using a conventional path, we find the crystalline bilayer does not self-assemble for $\Delta > 5\%$ polydispersity. For $\Delta > 3\%$, the amount of simulation time required to self-assemble the crystalline bilayer noticeably increased. Using the alternate path, the crystalline bilayer was stable up to 6%, and at low temperature a stable crystal/liquid phase was present until 12%. Multiple runs with different random starting distributions all showed a nearly identical response to a quasi-equilibrated increase in Δ. The coexistence phase found by the AP cannot be caused by traditional dispersity fractionation processes, which are kinetically slow and unlikely to be observed in simulation.[52,53] Rather, we are likely observing local regions with lattice defects or higher polydispersity spontaneously losing their crystalline ordering, while local regions without lattice defects and lower polydispersity do not. We note that in the portion of the CP and AP phase diagrams where the same phase is predicted (e.g., $\Delta < 5\%$ and $\Delta > 12\%$ Δ), all measurements were identical. In an experimental realization of this system with access to longer equilibration times, the coexistence of liquid and crystalline lamellar phases may be found, or the kinetics may be similarly limited.

V. CONCLUSIONS

In Ref. 38, we concluded that a small amount of polydispersity ($\Delta = 5\%$) encourages the formation of the DG phase, but a large amount ($\Delta > 10\%$) may kinetically prevent the phase from forming. In this paper, for the H and PLH phases, we conclude that there is no terminal polydispersity. Considering as high as $\Delta = 30\%$, these two phases were found to be present in both the CP and AP phase diagrams. The AP phase diagram, however, suggests that above a threshold polydispersity for each phase, the T^*_{ODT} may decrease with increasing Δ. We find a minimal amount of polydispersity ($\Delta = 6\%$ –12%) may be necessary to stabilize the PLH phase. For the L phase, we find that the crystalline bilayer phase has a terminal

polydispersity of ≈6%. For $6\% < \Delta < 12\%$, an L/PLH coexistence region or the PLH phase may be present. One consequence of the minimal and terminal polydispersity ranges identified above is that a manufactured population of TNS at a given polydispersity value may not be able to stably form all the ordered phases by simply changing ϕ.

The use of the alternate path, AP, phase diagram proves a useful way to study perturbations to a phase diagram. In this case, the perturbation was NS polydispersity. Rather than independently self-assembling perturbed systems, self-assembled ordered systems can be slowly adjusted to the perturbed state. In the case of polydispersity, this easily allows the impact of the perturbation to be studied continuously. Compared to CP phase diagrams, or phase diagrams generated by self-assembly from a disordered system, we found the AP method to reproduce the same phase boundaries with some small deviations. Even features particular to the CP phase diagram, such as the larger PLH region, can be reproduced by the AP method by considering an AP phase diagram where the polydispersity is increased to a terminal value, and then decreased again. This method is most valuable for studying phases that are difficult to self-assemble for kinetic reasons, such as the DG phase or the L/PLH coexistence region.

More generally, it is apparent that polydispersity can have subtle but important impacts on the properties of sphere packing, especially in unusual domain geometries. A relatively small amount of polydispersity can disrupt internal structures and change the per-particle energy of the packing. The local packing character of the nanoparticles was the dominant consideration in determining how polydispersity influenced the properties of the phase. In general, the phases with the more disordered packing were more tolerant of polydispersity than the more ordered phases. For sensitive phases that occupy a narrow volume fraction range of the phase diagram, such as the DG phase, or phases that occupy a wide volume fraction range but with internal crystalline ordering, such as the L phase, it can be critical to consider how much polydispersity a phase can tolerate before assuming the phase will be found in experimental systems.

ACKNOWLEDGMENTS

We thank Chris Rycroft for providing his Voronoi cell software that we then modified for use in this work and for providing helpful comments on the development of the polydisperse Voronoi methods. The 3D Voronoi Cell Software Library, Voro++, can be downloaded from http://math.lbl.gov/voro++/. We thank Joshua Anderson in the Glotzer group for his help with Hoomd-blue. HOOMD-blue can be downloaded from http://codeblue.umich.edu/hoomd-blue/. Research supported by the U.S. Department of Energy (DOE), Office of Basic Energy Sciences, Division of Materials Sciences and Engineering under Award No. DEFG02-02ER46000. C.L.P. also acknowledges the DOE Computational Science Graduate Fellowship under DOE Grant No. DE-FG02-97ER25308. We thank the University of Michigan Center for Advanced Computing for support of our computer clusters. We are grateful to National Center for Supercomputing Applications (NCSA) and National Energy Research Scientific Computing Center (NERSC) for computer time.

APPENDIX A: TECHNICAL DETAILS

In this Appendix, we provide more details and discussion on the methodological techniques introduced in Sec. II. In Sec. A 1 of Appendix A, we provide details about the functional form of the pair potentials used to model TNSs. In Sec. A 2 of Appendix A, we discuss how a distribution of polydisperse NS of polydispersity Δ is generated and in Sec. A 3 of Appendix A, we discuss how Δ can be continuously changed during a simulation. In Sec. A 4 of Appendix A, we further discuss the use of AP and CP thermodynamic paths to explore a phase diagram and in Sec. A 5 of Appendix A, we discuss the use of a slowly changing Δ to explore a phase diagram.

1. SLJ and WCA model for polydisperse tethered NS

For the coarse-grained molecular model described in Sec. II A, solvent selectivity is modeled by assuming that at sufficiently low T the solvent is poor for the NS but good for the tethers, resulting in a condition where nanoparticles will tend to aggregate.

The attraction between two nanoparticles of diameters d_i and d_j is modeled using a radially shifted 12-6 Lennard-Jones potential (LJ), which is also truncated and shifted to zero at r_{cutoff},

$$U_{\mathrm{LJS}} = \begin{cases} 4\epsilon\left(\left(\frac{\sigma}{r-\alpha_{ij}}\right)^{12} - \left(\frac{\sigma}{r-\alpha_{ij}}\right)^{6}\right) & \\ \quad -4\epsilon\left(\left(\frac{\sigma}{2.5}\right)^{12} - \left(\frac{\sigma}{2.5}\right)^{6}\right) & r < r_{cutoff} \\ 0 & r \geq r_{cutoff}, \end{cases} \tag{A1}$$

where, $r_{cutoff} = 2.5\sigma + \alpha_{ij}$ and $\alpha_{ij} = (d_i + d_j)/2 - \sigma$. The effect of the radially shifted Lennard-Jones potential is to fix the range of the potential and location of the attractive well with respect to the NS surface; the potential well minimum is the same distance from the surface of the NS for all sizes of NS. If the attraction between particles is the result of solvent selectivity, then this functional form is a reasonable assumption, as attraction will be a short ranged interaction not strongly affected by small changes in the particle size.

Solvophilic tethers interact via a purely repulsive WCA soft-sphere potential[40] to account for short-range, excluded volume interactions,

$$U_{\mathrm{WCA}} = \begin{cases} 4\epsilon\left(\left(\frac{\sigma}{r-\alpha_{ij}}\right)^{12} - \left(\frac{\sigma}{r-\alpha_{ij}}\right)^{6}\right) & \\ \quad +\epsilon & r < r_{cutoff} \\ 0 & r \geq r_{cutoff}, \end{cases} \tag{A2}$$

where $d_i = d_j = \sigma$ (that is, $\alpha_{ij} = 0$) and $r_{cutoff} = 2^{1/6}\sigma + \alpha_{ij}$. NS-tether interactions are also treated with the purely repulsive WCA soft-sphere potential to account for short-range, excluded volume interactions, modeled using Eq. (A2) with $d_{tether} = \sigma$ and $r_{cutoff} = 2^{1/6}\sigma + \alpha_{ij}$.

The natural units of this system are σ, the diameter of the tether bead; m_{tether}, the mass of a tether bead; and ε, the

Lennard-Jones well depth. Bulk system volume fraction, ϕ, is defined as the ratio of volume of the beads to the system volume, the dimensionless time is $t^* = \sigma\sqrt{m/\epsilon}$, and the degree of immiscibility and solvent quality are determined by the dimensionless temperature, $T^* = k_B T/\epsilon$, where T is fixed at 1.0 or ϵ is fixed at 1.0.

2. Polydisperse NS distributions

A set of polydisperse NS is created by sampling from a Gaussian distribution of particle diameters d,

$$P(d) = \frac{1}{\delta\sqrt{2\pi}}\exp\left[-\frac{1}{2}\left(\frac{d-\bar{d}}{\delta}\right)^2\right]. \quad \text{(A3)}$$

The non-dimensionalized polydispersity, Δ, is defined as $100\delta/\bar{d}$, where δ is the standard deviation and $\bar{d}$ is the average diameter. The population of diameters is then shifted or scaled so that the net volume of the nanoparticles is kept constant in order to prevent the bulk system volume fraction from deviating as polydispersity is introduced. The diameter distribution is also truncated at a minimum value of 1.0 so that all the NS are at least as large as a tether bead. The NS are polydisperse in size only. The mass of each nanoparticle is kept fixed at $m_{\mathrm{NS}} = 27m_{tether}$ to minimize the number of variables in the system.

3. Adjusting Δ

The simulation system sizes studied are large enough that polydispersity can be considered a global system variable. To change the polydispersity, the diameters of every particle in the system is adjusted only a small amount per time step to prevent high energy particle overlaps from occurring. Also, at each time step, the net volume of all the particles is kept fixed so ϕ remains constant as Δ is changed.

To accomplish this, the diameter of each particle i is made a monotonically increasing or decreasing function of λ, $d_i(\lambda)$, where $\lambda \in [0, 1]$ and the set of functions $\{d_i\}$ satisfy a constant volume constraint or

$$\sum_i^N \frac{d_i(\lambda)^3\pi}{6} = V_0. \quad \text{(A4)}$$

The polydispersity thus becomes a function of λ, where

$$\Delta(\lambda) = \frac{100\hat{\delta}(\{d_i(\lambda)\}}{\hat{\mu}(\{d_i(\lambda)\})}, \quad \text{(A5)}$$

where $\hat{\delta}$ and $\hat{\mu}$ are the standard deviation and mean of the set of diameters, respectively. In practice, a target distribution $\{d_i(\lambda = 1)\}$ at a given target polydispersity (e.g., 30%) is generated. Then at interim points, $0 < \lambda < 1$, a set of diameters are generated using linear interpolation between initial and final diameter for each particle. The set is then uniformly shifted or scaled at each interim point to satisfy the volume constraint. Other constraints, such as a minimum NS diameter, can then be imposed, but may necessitate multiple iterations before all constraints are satisfied. Polydispersity can then be changed by adjusting λ by small increments to the interim points.

4. Using CP and AP to bound the phase diagram

A diagram of an example of a CP and AP is shown in Figure 5. For both paths, simulations are initiated at a high temperature disordered monodisperse NS state. For a conventional path, we first slowly adjust the diameters of the NS to a polydisperse distribution. As the change to the diameters is performed while the system is hot, diffusive, and disordered, the state of the simulation when the polydisperse distribution is reached is indistinguishable from a simulation initialized with a polydisperse NS distribution. The simulation is then cooled via a cooling schedule to avoid kinetically trapped states. In studies of self-assembly using molecular dynamics (including BD), using a cooling schedule from a hot disordered state is a standard way the ordered phases of phase diagrams are generated. Cooling a system from a disordered state also emulates how physical particles self-assemble into an ordered state. Usually, when an ordered state is produced repeatedly, by different cooling schedules, or for different simulation sizes, cooling from a disordered state is considered to have produced the free energy minimizing state point. However, for kinetic reasons, or due to sensitivity of a phase to simulation box size, the free energy minimizing phase for a given state point may not be found in simulation.

In this paper, we will compare the phase diagram generated by the CP to an alternate thermodynamic path (AP). For the AP, we start with a monodisperse disordered high temperature system at a given ϕ. The temperature is lowered by a cooling schedule to a $T^* < T^*_{\mathrm{ODT}}$, so that the system is in the monodisperse ordered phase. In practice, only simulations with a minimal amount of defects in the ordered phase are retained for the next step. Polydispersity of the NS is then slowly increased to the desired Δ. The simulation is then heated via a schedule to a desired T^*.

The AP provides a different thermodynamic path for approaching a state point. For phases that are challenging to self-assemble (e.g., the DG phase), an advantage of the AP over the CP is that many independent simulations of the ordered phase at a given Δ, ϕ, and T^* can be rapidly and reliably generated. The sensitive phase may self-assemble only rarely using a CP method. The disadvantage of the AP is that it provides no information as to kinetic difficulty in forming the ordered phase from a disordered state.

5. Low temperature response to slowly changing the polydispersity

Phillips *et al.*[38] introduced a method for calculating the properties of a system as a continuous function of Δ without requiring a large number of computationally intensive independent CP simulations at fixed values of Δ intervals. To study Δ as a continuous variable, polydispersity is continuously added to the NS extremely slowly, or quasi-statically. The polydispersity is changed slowly enough that the system is able to relax in response to the change and the properties of the system, (barring kinetically trapped phase transition regions) calculated as a function of time, closely approximate those of the equilibrated system.

Staring with an ordered monodisperse system at $T^* = 0.25$ (i.e., H, DG, and L phases), the polydispersity of the NS is slowly increased (e.g., 0.3% $\delta\Delta/\times 10^6$ time steps) until a target $\Delta = 30\%$ is reached. This path through the phase diagram is referred to as quasiequilibrated Δ increasing, (QE$\Delta\uparrow$). Then the polydispersity is decreased at the same rate until the system is monodisperse. This path through the phase diagram is referred to as quasiequilibrated Δ decreasing, (QE$\Delta\downarrow$). The two paths (QE$\Delta\uparrow$ and QE$\Delta\downarrow$) used are illustrated in Figure 6. The simulation is thermostated to a low temperature $T^* = 0.25$ over the entire evolution. Properties, calculated as a function of time, closely approximate those of a CP or AP equilibrated system for a given polydispersity. In regions at $T^* = 0.25$ where the CP and AP phase diagrams differ, the properties calculated by the QE$\Delta\uparrow$ compare favorably to the AP system and properties calculated by the QE$\Delta\downarrow$ compare favorably to the CP system. If, at a given Δ, the system undergoes a phase transition via nucleation and growth, then this quasi-static method will generally fail to reproduce the equilibrated properties of the system except in the limit where the rate of changing Δ per time step approaches zero. Regions where the quasi-static method fails for this reason are indicated.

Another reason this method is superior to collecting and averaging a large number of computationally intensive independent CP simulations at fixed Δ values is the degeneracy found between independent simulations of ordered phases due to finite-size effects. For the H, L, and PLH phases, which do not have triply periodic unit cells, finite simulation sizes allow for the phase to arrange itself inside the simulation box in more than one way (e.g., orientation, distribution of perforations), and at slightly different energies. These differences should disappear at the thermodynamic limit. The self-assembled L phase is also susceptible to bilayer crystal defects, which should also disappear at the thermodynamic limit, but introduce slight energy differences between simulations.

These structural differences between different simulations of the same ordered phase confound the determination of the influence of polydispersity. However, if independent CP polydisperse systems are evolved along a QE$\Delta\downarrow$ path to obtain a desired property value at $\Delta = 0$, the systems all follow identical curves relative to the monodisperse value. The quasi-static method, therefore, correctly captures the perturbation polydispersity introduces to properties of the system at its monodisperse thermodynamic limit. The potential energy, packing fraction, and coordination are thus reported as offsets from the $\Delta = 0$ value. This also allows these properties to be more directly compared across volume fractions, ϕ.

APPENDIX B: ANALYSIS TECHNIQUES

1. R_{YLM} local structure analysis

In this Appendix, we discuss the use of R_{YLM} local structure analysis and Voronoi or radical tessellation in more detail in Secs. B 1 and B 2, respectively. To analyze the local configurations of the nanospheres, we performed the R_{YLM} local structure analysis first introduced in Iacovella *et al.*[24] and further discussed in Refs. 25 and 38. The R_{YLM} method relies on creating a rotationally invariant spherical harmonic fingerprint of the central particle of a cluster of particles (for harmonics l = 4, 6, 12) and then matching this fingerprint to a library of known structures. A cluster is identified as the reference configuration that minimizes the residual value, R, where $R = \sqrt{\sum_{i=4}^{12}(Q_i - Q_{ref})^2 + \sum_{i=4}^{12}(w_i - w_{ref})^2}$, or it is classified as disordered if it exceeds a certain cutoff. In the definition of R, Q_i, and w_i are two metrics of local ordering based on evaluating a set of spherical harmonic functions $Y_{lm}(\theta, \phi)$ and defined in Steinhardt *et al.*[54] For our system, the local packing of nanospheres is divided into clusters by grouping each NS and its nearest-neighbor nanospheres. Nearest neighbors are considered to be those with a surface-to-surface distance less than or equal to 0.5, such that each neighbor would be within the potential well of the central NS. In turn, each NS in the system is considered as a central NS to determine the distribution of cluster types. This method characterizes the bond angles in the local structures rather than the radial distance.

The R_{YLM} method permits recognition of the fact that the internal structure of a domain may be composed of many different local structures, not just one dominant structure type. In general, local structures are characterized by the family to which they belong, namely, icosahedral, crystalline, or disordered. Each family of structure types contains multiple reference structures with different coordination numbers. To characterize local icosahedral packing, we incorporated into our reference database a series of partial icosahedral clusters that maintain the same bond angles as the full icosahedral cluster, but with 0–4 particles removed. These local structures are almost identical to the LJ minimum potential energy clusters found by Wales and Doye,[55] which were also included in the reference database. The local structure is considered to be icosahedral if it matches the partial clusters from Wales and Doye[55] or a partial icosahedral cluster.

The library also includes a family of crystalline structures composed of full and partial coordination clusters with face-centered-cubic and hexagonal-close-packed bond angles.

The local structure of the DG was analyzed at $T^* = 0.25$ with a residual cutoff of $\sqrt{0.1} \approx 0.316$. Any cluster with a R value greater than 0.316 is considered disordered.

2. Voronoi and radical tessellation

The Voronoi tessellation is a useful tool for extracting measurable properties from a system of particles. The Voronoi cell around a point is generally defined as the region of space that is closer to the given point than any other point. In a three-dimensional space, the Voronoi cells for a set of points uniquely divides, or tessellates, the space into irregular polyhedra with flat faces and straight edges. If each point is the center of a spherical particle in a system of non-overlapping monodisperse spheres, then each sphere is completely contained within its Voronoi cell. The volume fraction of the

sphere inside its Voronoi cell has been proposed as a local measure of density[56] and the shared facets of a cell define the neighbors. However, for polydisperse spheres, a standard Voronoi tessellation is no longer a suitable tessellation since it is possible for a sphere to overlap the boundary of its cell. Phillips *et al.*[38] proposed using a radical tessellation, an extension of the Voronoi tessellation, to study the packing of the polydisperse spheres. Like the Voronoi tessellation, the radical tessellation also decomposes space into cells that are irregular polyhedra with flat faces and straight edges. But, as long as the set of polydisperse spheres do not overlap each other, each sphere is completely contained inside its radical cell. Reference 57 further discusses how the radical tessellation method can be used to study phase separated soft matter systems with complicated geometries. For example, by measuring the packing density of the tether domain of a TNS system, we can verify that the tethers are well away from the glass transition and not dominating the kinetics of the self-assembly process.[58,59]

[1] C. Park, J. Yoon, and E. L. Thomas, "Enabling nanotechnology with self assembled block copolymer patterns," Polymer **44**(22), 6725–6760 (2003).
[2] T. P. Lodge, "Block copolymers: Past successes and future challenges," Macromol. Chem. Phys. **204**(2), 265–273 (2003).
[3] M. J. Fasolka and A. M. Mayes, "Block copolymer thin films: Physics and applications," Annu. Rev. Mater. Res. **31**, 323–355 (2001).
[4] C. T. Black, K. W. Guarini, R. Ruiz, E. M. Sikorski, I. V. Babich, R. L. Sandstrom, and Y. Zhang, "Polymer self assembly in semiconductor microelectronics," IBM J. Res. Dev. **51**(5), 605–633 (2007).
[5] M. P. Stoykovich and P. F. Nealey, "Block copolymers and conventional lithography," Mater. Today **9**(9), 20–29 (2006).
[6] J. Yoon, W. Lee, and E. L. Thomas, "Self-assembly of block copolymers for photonic-bandgap materials," MRS Bull. **30**(10), 721–726 (2005).
[7] Y. Fink, A. M. Urbas, M. G. Bawendi, J. D. Joannopoulos, and E. L. Thomas, "Block copolymers as photonic bandgap materials," J. Lightwave Technol. **17**(11), 1963–1969 (1999).
[8] B. Jeong, Y. H. Bae, D. S. Lee, and S. W. Kim, "Biodegradable block copolymers as injectable drug-delivery systems," Nature (London) **388**(6645), 860–862 (1997).
[9] G. S. Kwon, "Block copolymer micelles as drug delivery systems," Adv. Drug Delivery Rev. **54**(2), 167–167 (2002).
[10] Z. L. Zhang, M. A. Horsch, M. H. Lamm, and S. C. Glotzer, "Tethered nano building blocks: Toward a conceptual framework for nanoparticle self-assembly," Nano Lett. **3**(10), 1341–1346 (2003).
[11] M. A. Horsch, Z. L. Zhang, and S. C. Glotzer, "Self-assembly of polymer-tethered nanorods," Phys. Rev. Lett. **95**(5), 056105 (2005).
[12] S. C. Glotzer, M. A. Horsch, C. R. Iacovella, Z. Zhang, E. R. Chan, and X. Zhang, "Self-assembly of anisotropic tethered nanoparticle shape amphiphiles," Curr. Opin. Colloid Interface Sci. **10**(5–6), 287–295 (2005).
[13] S. C. Glotzer and M. J. Solomon, "Anisotropy of building blocks and their assembly into complex structures," Nature Mater. **6**, 557–562 (2007).
[14] T. B. Martin, A. Seifpour, and A. Jayaraman, "Assembly of copolymer functionalized nanoparticles: A Monte Carlo simulation study," Soft Matter **7**, 5952–5964 (2011).
[15] A. Jayaraman and K. S. Schweizer, "Structure and assembly of dense solutions and melts of single tethered nanoparticles," J. Chem. Phys. **128**(16), 164904 (2008).
[16] A. Jayaraman and K. S. Schweizer, "Effective interactions, structure, and phase behavior of lightly tethered nanoparticles in polymer melts," Macromolecules **41**(23), 9430–9438 (2008).
[17] S. Westenhoff and N. A. Kotov, "Quantum dot on a rope," J. Am. Chem. Soc. **124**(11), 2448–2449 (2002).
[18] K.-M. Sung, D. W. Mosley, B. R. Peelle, S. Zhang, and J. M. Jacobson, "Synthesis of monofunctionalized gold nanoparticles by fmoc solid-phase reactions," J. Am. Chem. Soc. **126**(16), 5064–5065 (2004).
[19] F. Huo, A. K. R. Lytton-Jea, and C. A. Mirkin, "Asymmetric functionalization of nanoparticles based on thermally addressable dna interconnects," Adv. Mater. **18**(17), 2304–2306 (2006).
[20] J. G. Worden, A. W. Shaffer, and Q. Huo, "Controlled functionalization of gold nanoparticles through a solid phase synthesis approach," Chem. Commun. **2004**(5), 518–519.
[21] G. A. DeVries, M. Brunnbauer, Y. Hu, A. M. Jackson, B. Long, B. T. Neltner, O. Uzun, B. H. Wunsch, and F. Stellacci, "Divalent metal nanoparticles," Science **315**(5810), 358–361 (2007).
[22] F. A. Aldaye and H. F. Sleiman, "Dynamic DNA templates for discrete gold nanoparticle assemblies: Control of geometry, modularity, write/erase and structural switching," J. Am. Chem. Soc. **129**(14), 4130–4131 (2007).
[23] C. R. Iacovella, M. A. Horsch, Z. Zhang, and S. C. Glotzer, "Phase diagrams of self-assembled mono-tethered nanospheres from molecular simulation and comparison to surfactants," Langmuir **21**(21), 9488–9494 (2005).
[24] C. R. Iacovella, A. S. Keys, M. A. Horsch, and S. C. Glotzer, "Icosahedral packing of polymer-tethered nanospheres and stabilization of the gyroid phase," Phys. Rev. E **75**(4), 040801 (2007).
[25] C. R. Iacovella and S. C. Glotzer, "Local ordering of polymer-tethered nanospheres and nanorods," J. Chem. Phys. **129**, 044902 (2008).
[26] F. J. Martinez-Veracoechea and F. A. Escobedo, "Lattice Monte Carlo simulations of the gyroid phase in monodisperse and bidisperse block copolymer systems," Macromolecules **38**(20), 8522–8531 (2005).
[27] D. A. Hajduk, P. E. Harper, S. M. Gruner, C. C. Honeker, G. Kim, E. L. Thomas, and L. J. Fetters, "The gyroid – A new equilibrium morphology in a weakly segregated diblock copolymers," Macromolecules **27**(15), 4063–4075 (1994).
[28] M. A. Horsch, Z. L. Zhang, C. R. Iacovella, and S. C. Glotzer, "Hydrodynamics and microphase ordering in block copolymers: Are hydrodynamics required for ordered phases with periodicity in more than one dimension?," J. Chem. Phys. **121**(22), 11455–11462 (2004).
[29] M. M. Maye, W. X. Zheng, F. L. Leibowitz, N. K. Ly, and C. J. Zhong, "Heating-induced evolution of thiolate-encapsulated gold nanoparticles: A strategy for size and shape manipulations," Langmuir **16**(2), 490–497 (2000).
[30] M. Y. Ge, H. P. Wu, L. Niu, J. F. Liu, S. Y. Chen, P. Y. Shen, Y. W. Zeng, Y. W. Wang, G. Q. Zhang, and J. Z. Jiang, "Nanostructured ZnO: From monodisperse nanoparticles to nanorods," J. Cryst. Growth **305**(1), 162–166 (2007).
[31] W. L. Pei, S. Kakibe, I. Ohta, and M. Takahashi, "Controlled monodisperse Fe nanoparticles synthesized by chemical method," IEEE Trans. Magn. **41**(10), 3391–3393 (2005).
[32] P. G. Bolhuis and D. A. Kofke, "Monte Carlo study of freezing of polydisperse hard spheres," Phys. Rev. E **54**(1), 634–643 (1996).
[33] P. N. Pusey, "The effect of polydispersity of the crystalization of hard spherical colloids," J. Phys. **48**, 709–712 (1987).
[34] P. N. Pusey, "Colloidal suspensions," in *Les Houches Session L1: Liquids, Freezing, and the Glass Transition*, edited by J. P. Hansen, D. Levesque, and J. Zinn-Justin (North-Holland, 1991), pp. 765–942.
[35] F. M. van der Koolj, K. Kassapidou, and H. N. W. Lekkerkerker, "Liquid crystal phase transition in suspensions of polydisperse plate-like particles," Nature (London) **406**, 868–871 (2000).
[36] R. P. Sear, "Phase separation and crystallisation of polydisperse hard spheres," Europhys. Lett. **44**(4), 531–535 (1998).
[37] M. A. Bates and D. Frenkel, "Influence of polydispersity on the phase behavior of colloidal liquid crystals: A Monte Carlo simulation study," J. Chem. Phys. **109**, 6193–6199 (1998).
[38] C. L. Phillips, C. R. Iacovella, and S. C. Glotzer, "Stability of the double gyroid phase to nanoparticle polydispersity in polymer-tethered nanosphere systems," Soft Matter **6**, 1693–1703 (2010).
[39] G. S. Grest and K. Kremer, "Molecular-dynamics simulation for polymers in the presence of a heat bath," Phy. Rev. A **33**(5), 3628–3631 (1986).
[40] J. D. Weeks, D. Chandler, and H. C. Andersen, "Role of repulsive forces in determining the equilibrium structure of simple liquids," J. Chem. Phys. **54**(12), 5237–5247 (1971).
[41] M. Yiannourakou, I. G. Economou, and I. A. Bitsanis, "Phase equilibrium of colloidal suspensions with particle size dispersity: A Monte Carlo study," J. Chem. Phys. **130**(19), 194–902 (2009).
[42] L. Santen and W. Krauth, "Liquid, glass and crystal in two-dimensional hard disks," e-print arXiv:cond-mat/0107459v1.
[43] S. Pronk and D. Frenkel, "Melting of polydisperse hard disks," Phys. Rev. E **69**(6), 066123 (2004).

[44]M. Maldovan, A. M. Urbas, N. Yulfa, W. C. Carter, and E. L. Thomas, "Photonic properties of bicontinuous cubic microphases," Phys. Rev. B **65**(16), 165123 (2002).
[45]M. R. Sadr-Lahijany, P. Ray, and H. E. Stanley, "Dispersity-driven melting transition in two-dimensional solids," Phys. Rev. Lett. **79**(17), 3206–3209 (1997).
[46]D. A. Kofke and P. G. Bolhuis, "Freezing of polydisperse hard spheres," Phys. Rev. E **59**(1), 618–622 (1999).
[47]N. B. Wilding and P. Sollich, "Phase behavior of polydisperse spheres: Simulation strategies and an application to the freezing transition," J. Chem. Phys. **133**(22), 224102 (2010).
[48]S. Auer and D. Frenkel, "Suppression of crystal nucleation in polydisperse colloids due to increase of the surface free energy," Nature (London) **413**(6857), 711–713 (2001).
[49]P. Bartlett, "Freezing in polydisperse colloidal suspensions," J. Phys.: Condens. Matter **12**(8A), A275–A280 (2000).
[50]L. A. Fernández, V. Martín-Mayor, and P. Verrocchio, "Phase diagram of a polydisperse soft-spheres model for liquids and colloids," Phys. Rev. Lett. **98**(8), 085702 (2007).
[51]S. Martin, G. Bryant, and W. van Megen, "Observation of a smecticlike crystalline structure in polydisperse colloids," Phys. Rev. Lett. **90**(25), 255702 (2003).
[52]H. J. Schöpe, G. Bryant, and W. van Megen, "Two-step crystallization kinetics in colloidal hard-sphere systems," Phys. Rev. Lett. **96**(17), 175701 (2006).
[53]S. Martin, G. Bryant, and W. van Megen, "Crystallization kinetics of polydisperse colloidal hard spheres: Experimental evidence for local fractionation," Phys. Rev. E **67**(6), 061405 (2003).
[54]P. J. Steinhardt, D. R. Nelson, and M. Ronchetti, "Bond-orientational order in liquids and glasses," Phys. Rev. B **28**(2), 784–805 (1983).
[55]D. J. Wales and J. P. K. Doye, "Global optimization by basin-hopping and the lowest energy structures of Lennard-Jones clusters containing up to 110 atoms," J. Phys. Chem. A **101**(28), 5111–5116 (1997).
[56]C. H. Rycroft, G. S. Grest, J. W. Landry, and M. Z. Bazant, "Analysis of granular flow in a pebble-bed nuclear reactor," Phys. Rev. E **74**(2), 021306 (2006).
[57]C. L. Phillips and S. C. Glotzer, "Voronoi tessellation for characterizing microphase separated soft matter systems," preprint.
[58]F. Puosi and D. Leporini, "Spatial displacement correlations in polymeric systems," J. Chem. Phys. **136**(16), 164901 (2012).
[59]A. Ottochian and D. Leporini, "Universal scaling between structural relaxation and caged dynamics in glass-forming systems: Free volume and time scales," J. Non-Cryst. Solids **357**(2), 298–301 (2011).